Korean J. Chem. Eng., 39(5), 1287-1298 (2022)
DOI: 10.1007/s11814-021-1030-y

pISSN: 0256-1115
eISSN: 1975-7220

Response surface analysis of energy balance and optimum condition for torrefaction of corn straw

Shuai Guo, Tiankuo Guo, Deyong Che, Hongpeng Liu, and Baizhong Sun†

School of Energy and Power Engineering, Northeast Electric Power University, Jilin 132012, China
(*Received 14 August 2021 • Revised 4 November 2021 • Accepted 29 November 2021*)

Abstract−Corn straw has potential as a biofuel, and is generated in large amounts globally. However, this potential remains underutilized, and torrefaction is one of the processes that can be implemented to improve the energy grade of this biomass. In this study, three process parameters (temperature, heating rate, residence time) were investigated using a response surface method to optimize the torrefaction process of corn straw. At 242.26 °C, a 60 min residence time, and 6.28 °C/min heating rate, the mass yield and higher heating value (HHV) reached their maximum values. Temperature was the most important factor influencing torrefaction, followed by residence time and then heating rate. The gas and liquid by-products were measured by mass spectrometry and mass spectrometry-gas chromatography, and the heat demand of torrefaction was measured by thermogravimetric analysis-differential scanning calorimetry. The HHV of the by-products changed little before 240 °C but increased considerably as the temperature further increased. The HHV at 242 °C was 1,273 kJ/kg. When the heat loss was 50%, 242 °C was the critical point of energy balance, and after that the torrefaction process was energy self-sufficient. These findings provide data to support the establishment of semi-industrial or industrial corn straw torrefaction devices.

Keywords: Torrefaction, Biomass Energy, Response Surface Method, Corn Straw, Energy Balance

INTRODUCTION

The depletion of fossil fuels and the greenhouse effect, haze, and pollution caused by their combustion for transportation and energy production have attracted the attention of scientists and the general public worldwide. In this context, solar, wind, water, geothermal energy, and other environmentally friendly renewable energy sources have become increasingly important as alternatives to fossil fuels [1]. Biomass is the fourth largest energy source worldwide after coal, oil, and natural gas, and its advantages include a high storage capacity and low cost [2]. Moreover, as biomass materials are derived from the photosynthesis of water and CO_2, they are considered carbon neutral. Biomass combustion produces less NO_x and SO_x than coal combustion [3]. However, biomass also has a high moisture content, poor hygroscopicity, poor grindability, and low calorific value, which lead to inconvenient transportation and storage [4]. Corn straw is a biomass material, and the world's production of this waste is approximately 2 billion tons per year [5]. China's annual production of corn straw can reach 700 million tons [6], which accounts for approximately one-third of the global production. Despite its potential, corn straw is commonly disposed in landfills or incinerated. Thus, its potential is not fully utilized, resulting in a considerable waste of resources. Therefore, the potential for more effective use of corn straw should be explored.

The most common biomass treatments are physical, chemical, biological, and thermochemical conversion processes [7]. Physical transformation includes drying, crushing, granulation, and other physical processes. Chemical transformation includes mainly gasification and pressurized liquefaction. Biotransformation often includes the use of enzyme catalysts or microorganisms and thermochemical transformation, and it transforms biomass into a gas, liquid, or solid product through thermochemical reactions. Torrefaction is a type of thermochemical transformation that effectively improves the energy grade of biomass and facilitates thermochemical processes, such as gasification and liquefaction [8].

Torrefaction is a pretreatment method wherein biomass undergoes slow pyrolysis [9] in an inert atmosphere at 200-300 °C, a heating rate less than 30 °C/min, and a residence time less than 60 min [10]. After torrefaction, the H/C and O/C ratios and hemicellulose content of biomass decrease, whereas the cellulose, lignin, and ash content increase [11-13]. After torrefaction, the higher heating value (HHV) of biomass increases [14], water content decreases, hydrophobicity and grindability are improved, and its properties become closer to those of coal [15].

The main factors affecting torrefaction are the reaction temperature, heating rate, residence time, particle size, water content, and environmental pressure. Temperature is the most important factor because torrefaction can be divided into light (200-235 °C), mild (235-275 °C), and severe torrefaction (275-300 °C) [16]. As the temperature increases, the quality of the solid products decreases, and the proportion of liquid and gas products increases [17]. Halina et al. [18] investigated the importance of temperature in different scale reactors and observed that after torrefaction, the hydrophobicity and grindability of the biomass were enhanced and the HHV was improved. Sulaiman et al. [19] studied the torrefaction of empty fruit bunches at different temperature and residence time. Their results

†To whom correspondence should be addressed.
E-mail: sunbaizhong@126.com

showed that temperature was the most important factor affecting torrefaction, and the solid yield showed a downward trend with increasing residence time. Chiou et al. [20] reached the same conclusion in a study on pomaces and nut shells, in which an increase in the heating time and temperature led to a decrease in H/C and O/C. Li et al. [21] observed that with increasing temperature, the moisture absorption rate of pellets decreased, and the performance of the pellets was affected by the removal of most of the components with low melting point. Yu et al. [22] found that the mass yield and energy yield decreased with an increase in the temperature and oxygen concentration through experiments on corn straw in different atmospheres. Zhang et al. [23] discussed the effects of temperature and the K element on torrefaction, and they reported that a high torrefaction temperature under the catalytic action of K positively contributed to the char yield. Torrefaction in the presence of K decreases the O/C molar ratio and changes the pore structure of char. Ozben et al. [24] used a response surface method to study the torrefaction of cotton stalks and reported that the HHV reached 21.63 MJ/kg at 303.46 °C, a 60 min residence time, and 165.87 kg/m^3 bulk density. Singh et al. [25] optimized the energy yield and HHV of the torrefaction of *Acacia nilotica* at 252 °C, a 60 min residence time, and 5 °C/min heating rate.

Energy balance is a process in which the combustion heat obtained from the gaseous and liquid by-products during torrefaction can be used to provide energy for the torrefaction process, such that the entire process can achieve energy self-sufficiency without an external heat supply. To determine the energy balance of the torrefaction process, the energy of the gas and liquid products and the heat required for the torrefaction process should be measured or calculated. Granados et al. [26] studied the torrefaction of six different biomasses, among which sawdust was the most promising, with an HHV increase of 14.5%, whereas rice husks produced 1,541 kJ/kg of heat during the reaction. Bates et al. [27] modeled thermochemical reactions to simulate the mass and energy balances, and they concluded that in the first stage of exothermic heat, the formation of volatiles during torrefaction consumes heat, whereas the formation of tar releases heat, at 40-280 kJ/kg; meanwhile, in the second stage, exothermicity depends on temperature. Ferreira et al. [28] used thermogravimetric and differential scanning calorimetry (TG-DSC) to study sugarcane straw under different heating rates and atmospheres to obtain the heat required for pyrolysis. They reported that the heat absorption decreased from 466 to 182 kJ/kg as the heating rate increased from 5 to 20 K/min, and at a 3% O_2 atmosphere, the heat demand did not vary significantly. Singh et al. [29] studied the energy and exergy of the torrefaction of pea stalks and eucalyptus, and observed that the recovery of energy from liquid products could increase the solid energy recovery by 8-9%. Ohliger et al. [30] studied the heat demand and reaction heat of beechwood torrefaction, and observed that the heat demand per unit mass ranged from 249 to 986 J/g, and a higher residence time reduced the heat demand. Moreover, depending on different parameters, the reaction heat changed from slightly endothermic to slightly exothermic.

Most studies focus on the influencing factors of torrefaction and on the properties of torrefied solid products, energy balance, and heat of reaction. However, few studies have investigated the optimal torrefaction conditions, including the temperature, residence time, and heating rate of corn straw, but research on its energy balance under optimal torrefaction conditions has not been published. As mass yield (MY) and HHV show opposite trends during torrefaction processes, we used the response surface method to optimize three important factors: temperature, heating rate, and residence time. HHV and MY were the optimization targets. Energy densification and yield were comprehensively considered for the optimization of corn straw torrefaction conditions. Based on the optimized heating rate and residence time, experiments were conducted to determine the optimal temperature. The composition and content of the gas and liquid products from the torrefaction were examined by mass spectrometry (MS) and gas chromatography (GC-MS), respectively. The heat demand during torrefaction was determined by TG-DSC. Finally, the energy balance was established under the best torrefaction parameters of corn straw, and we designed a bench-scale torrefaction device based on the energy balance.

MATERIALS AND METHODS

1. Materials

The corn straw samples used in this study were harvested in Jilin province, China. They were air-dried, chopped into small pieces of 3-5 cm, dried at 105 °C for 24 h, and pulverized to a powder with particle size of 0-75 mm. The proximate and ultimate analyses of the samples are summarized in Table 1. The proximate analysis was performed based on the Chinese standard GB/T 212-2008 with an industrial analyzer (SDLA718, Hunan Sundy Science, China). The ultimate analysis for carbon, hydrogen, oxygen, nitrogen, and sulfur was conducted with an automatic elemental analyzer (EA3000, Euro Vector, Italy) according to the GB/T 30733-2014 standard.

2. Experimental Design

Box-Behnken design, a type of response surface methodology, is a global statistical model used to investigate and optimize the effect of three or more independent variables [31]. Temperature, heating rate, and residence time were chosen as the parameters. In total, 17 experiments were conducted considering a design with three factors and three levels, including five repetitions in the center point. The matrix of the experimental design is shown in Table 2.

The regression model feasibility was determined with a confidence level of 95% using analysis of variance (ANOVA). The effect of three independent variables was examined for every response,

Table 1. Proximate and ultimate analyses of corn straw samples

Proximate analyses/wt%				Ultimate analyses/wt%				
M_{ad}	A_{ad}	V_{ad}	FC_{ad}	C_{ad}	H_{ad}	O_{ad}	N_{ad}	S_{ad}
4.81	5.41	76.56	13.22	44.16	5.77	40.14	0.54	0.23

Table 2. Matrix of experimental design

No.	Temperature	Heating rate	Residence time
1	280	10.0	45
2	280	7.5	60
3	280	7.5	30
4	280	5.0	45
5	250	7.5	45
6	250	5.0	60
7	250	7.5	45
8	250	7.5	45
9	250	7.5	45
10	250	7.5	45
11	250	10.0	60
12	250	5.0	30
13	250	10.0	30
14	220	5.0	45
15	220	10.0	45
16	220	7.5	60
17	220	7.5	30
18	25	0	0

and the response surface was used to optimize the process [21]. To investigate the feasibility of the torrefied corn straw as a fuel, HHV, MY, and energy yield were chosen as responses. Mass and energy yields were calculated according to Eqs. (1) and (2) [32] as follows:

$$\text{Mass Yield} = \frac{\text{Weight of torrified biomass}}{\text{Weight of raw biomass}} \times 100\% \quad (1)$$

$$\text{Energy Yield} = \text{Mass Yield} \times \frac{\text{HHV of torrified biomass}}{\text{HHV of raw biomass}} \times 100\% \quad (2)$$

3. Experimental Setup and Analytical Methods

The schematic diagram of the experimental system is shown in Fig. 1. The torrefaction experiment was conducted in an argon atmosphere, wherein argon enters the reactor through a flow control device, the reactor temperature is controlled by three resistance wires connected to thermocouples, and the uncertainty is 1 °C. The gas and liquid by-products were separated using ice-water baths and measured thereafter.

Response surface methodology (RSM) is an experimental design method that is often used to optimize process conditions [33]. It overcomes the shortcomings of orthogonal design, in which the same factor only can be compared at different levels and the best combination of factors cannot be obtained in the whole search range. Box-Behnken is a commonly used model in the RSM and is usually an effective tool for optimization [34]. ANOVA is usually used in combination with the Box-Behnken design method to determine the accuracy of the model based on the p-value, F-value, and R^2, among others, and compare the influence of independent variables on dependent variables [35].

The temperature, heating rate, and residence time were determined by the response surface method. In each experiment, 5± 0.01 g of corn straw was loaded into the reactor, and argon was introduced at 400 mL/min for 30 min to ensure that the pre-existing air in the reactor was expelled. After adjusting the temperature, heating rate, and residence time, the gas produced by the torrefaction was cooled through second-stage condensation, which collected condensable gases and non-condensable components. The tar composition was measured by GC-MS (6890N/5975, Agilent, USA), and the non-condensable components were identified by MS (LC-D200M, USA). The HHV of biochar was measured by an oxygen bomb calorimeter (SDC311, Hunan Sundy Science, China).

To establish the energy balance of the torrefaction process, we calculated the combustion heat of the gas and liquid products and the heat required for the torrefaction process. We integrated the mass spectrum data to identify the mass ratio of each component in the non-condensable gas, and the HHV of gas was obtained based on the gas mass at different experimental temperatures. The

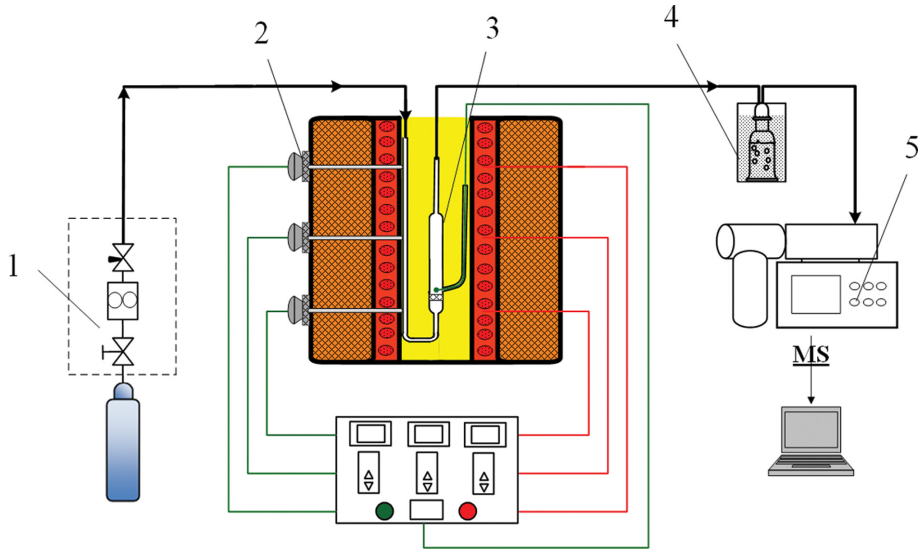

Fig. 1. Schematic diagram of the experimental system.
1. Flow control device 2. Thermocouple 3. Reactor 4. Ice-water bath 5. MS

main torrefaction gas products were H_2, CO, CO_2, CH_4, and N_2 [36-38]. The HHV of the gas was mainly provided by the CO, H_2, and CH_4. As the amount of H_2 produced during torrefaction was significantly small, the influence of H_2 was ignored when calculating the gas HHV. The specific calculation method was as follows [39]:

$$HHV_g = 10.11 m_{CO} + 50.02 m_{CH_4} \quad (3)$$

where HHV_g represents the HHV (kJ/g) of the gas product, which is 10.11 and 50.02 for CO and CH_4, respectively; m_{CO} and m_{CH_4} are the mass of CO and CH_4 produced from 1 kg of corn straw. Eq. (4) shows the calculation of HHV for different tar components, as follows:

$$HHV_x = \alpha \times A \quad (4)$$

where HHV_x is the heat of combustion of the x component of tar, α is the ratio of the peak area of x in the GC-MS to the total area, and A is the heat released by the complete combustion of x. The HHV contribution of each component was calculated, and their sum represents the combustion heat of tar at different temperatures.

RESULTS AND DISCUSSION

1. Analysis of Mass and Energy Yield

MY, energy yield, and calorific values of the corn straw samples are shown in Table 3. The HHV was 15,557.3 kJ/kg, whereas the mass loss and energy yield depended on the operation conditions. Table 3 shows that regardless of the residence time and heating rate, the MY of the corn straw decreased from 83.25% to 53.84% as the temperature increased from 220 to 280 °C. With the same heating rate and residence time, the MY decreased from 83.25% to 58.91% with increasing temperature. These results show that temperature is the main factor influencing torrefaction. For a constant temperature and residence time, the maximum and minimum difference in MY was 0.24% and 0.17%, respectively, and this difference increased with an increasing temperature. Given a constant temperature and heating rate, the maximum and minimum difference in MY with different residence times was 0.51% and 0.25% respectively, and this value also increased with increasing temperature. Therefore, temperature was the most important factor affecting the MY. MY decreased with increasing temperature, and energy yield showed the same trend [22]. Williams et al. [40] stated that when the pyrolysis temperature is low, there is competition between tar formation and carbonization. Regarding the heating rate, a slow heating rate could lead to a relatively prolonged residence time of volatiles, giving rise to higher carbon yields. At a faster heating rate, the coking reaction was inhibited and the tar output was reduced. The increase in residence time could also lead to an increase in liquid products because the devolatilization reaction time increases with an increasing residence time [41,42].

Table 3. Mass and energy yield under different conditions

No.	HHV (kJ/kg)	Mass yield (%)	Energy yield (%)
1	18,874.5	54.88	66.58
2	18,985.8	53.84	65.70
3	18,859.4	58.91	71.41
4	17,793.4	57.26	65.49
5	17,233.0	68.49	75.87
6	17,892.1	70.08	80.59
7	17,336.9	73.94	82.40
8	17,201.3	68.10	75.29
9	17,559.5	70.85	79.97
10	17,487.5	73.34	82.44
11	17,408.1	67.79	75.86
12	16,579.4	78.63	83.79
13	17,494.8	72.17	81.16
14	16,504.1	82.66	87.69
15	16,686.3	81.00	86.88
16	16,812.9	80.79	87.31
17	16,774.1	83.25	89.77
18	15,557.3	100	100

These changes were attributed to the decomposition reaction of the three components, including the dehydroxylation and decarboxylation of hemicellulose and the partial depolymerization and demethoxylation of cellulose and lignin [43]. For temperatures less than 200 °C, corn straw samples were mainly dehydrated, and a small amount of volatiles was removed. At 200 °C, hemicellulose begins to decompose, mainly through deacetylation and depolymerization reactions [44,45]. At this temperature, the amorphous phase of cellulose also begins to decompose along with part of the lignin demethoxylation (eugenol base) [46]. At approximately 250 °C, cellulose begins to degrade on a large scale, the cellulose crystal phase begins to decompose, and lignin undergoes depolymerization. At 300 °C, cellulose begins to degrade, the lignin fat side chains are cracked, and most hemicellulose is degraded [47].

2. Response Surface Analysis of HHV and MY of Biochar

2-1. Analysis and Verification of Model Equation

$$MY = 0.71 - 0.13A - 0.016B - 0.026C - 1.811\times10^{-3}AB - 6.509\times10^{-3}AC + 0.010BC - 0.025A^2 + 4.887\times10^{-3}B^2 + 7.34\times10^{-3}C^2 \quad (5)$$

$$HHV = 17{,}363.64 + 966.96A + 211.84B + 173.90C + 224.72AB + 21.90AC - 349.85BC + 307.69A^2 - 206.76B^2 + 186.72C^2 \quad (6)$$

To predict an adequate response, we used the original unit value of each factor. The Box-Behnken design method was used to arrange the experiment based on three factors and three levels. According to the second-order polynomial equation proposed by the central combination design, the least square method was used to fit the dependent variables. Thus, the coefficients are obtained by fitting the experimental values. Eqs. (5) and (6) are regression equation models of MY and HHV, respectively, where A, B, and C represent temperature, heating rate, and residence time, respectively. These equations provide the response values of corn straw torrefaction. The sign of the coefficients in the equation represents a promoting or suppressing effect exerted by the influencing factors on the response value: "+" represents a promoting effect, and "–" represents a suppressing effect. For the MY, all three influencing factors had an inhibitory effect under a single condition, and the product terms with temperature participation such as AB, AC, and A^2 also showed the same trend. The product terms of B and C (e.g., BC, B^2, C^2) all

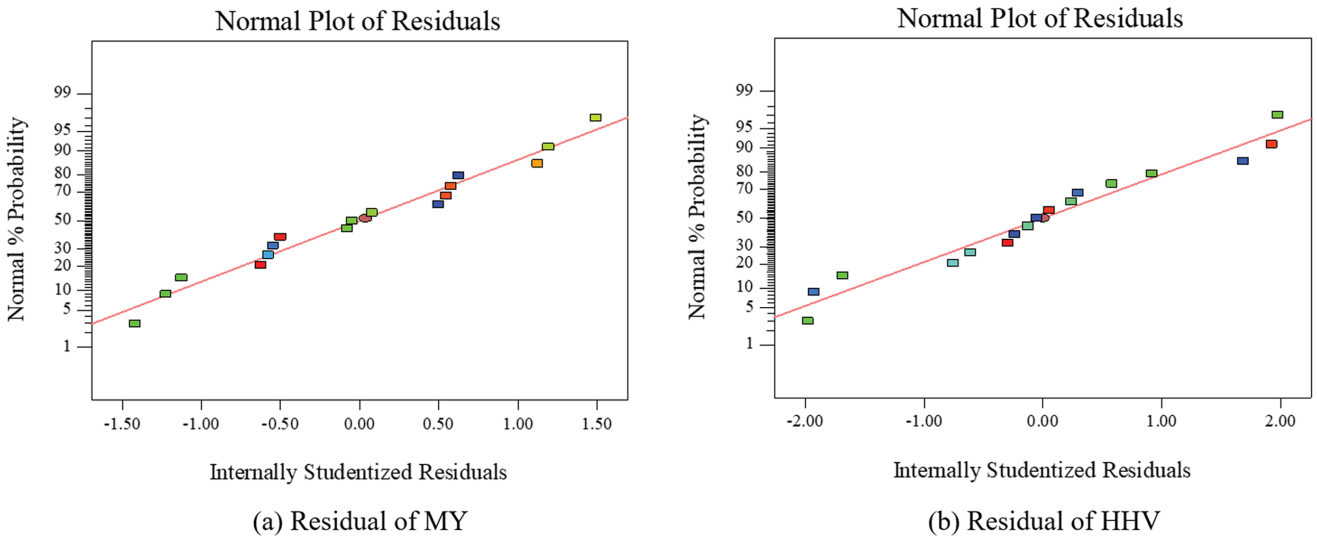

Fig. 2. Residual analysis of MY and HHV.

Table 4. ANOVA for quadratic response model of MY and HHV

MY					
	Sum of squares	df	Mean square	F-value	p-value
Model	0.14	9	0.016	31.49	<0.0001
A-temperature	0.13	1	0.13	262.15	<0.0001
B-rate	2.04×10^{-3}	1	2.04×10^{-3}	4.05	0.084
C-time	5.24×10^{-3}	1	5.24×10^{-3}	10.4	0.0146
AB	1.31×10^{-5}	1	1.31×10^{-5}	0.026	0.8764
AC	1.70×10^{-4}	1	1.70×10^{-4}	0.34	0.5802
BC	4.35×10^{-4}	1	4.35×10^{-4}	0.86	0.3839
A^2	2.59×10^{-3}	1	2.59×10^{-3}	5.14	0.0576
B^2	1.01×10^{-4}	1	1.01×10^{-4}	0.2	0.6686
C^2	2.27×10^{-4}	1	2.27×10^{-4}	0.45	0.5234
Residual	3.53×10^{-3}	7	5.04×10^{-4}		
Lack of Fit	6.41×10^{-4}	3	2.14×10^{-4}	3.00E-01	0.8275
Pure Error	2.89×10^{-3}	4	7.22×10^{-4}		
Cor Total	0.15	16			
HHV					
	Sum of squares	df	Mean square	F-value	p-value
Model	9.48×10^{-6}	9	1.05×10^{-6}	18.38	0.0004
A-temperature	7.48×10^{-6}	1	7.48×10^{-6}	130.51	<0.0001
B-rate	3.59×10^{-5}	1	3.59×10^{-5}	6.26	0.0408
C-time	2.42×10^{-5}	1	2.42×10^{-5}	4.22	0.079
AB	2.02×10^{-5}	1	2.02×10^{-5}	3.52	0.1026
AC	1,918.44	1	1,918.44	0.033	0.86
BC	4.90×10^{-5}	1	4.90×10^{-5}	8.54	0.0223
A^2	3.99×10^{-5}	1	3.99×10^{-5}	6.96	0.0336
B^2	1.80×10^{-5}	1	1.80×10^{-5}	3.14	0.1197
C^2	1.47×10^{-5}	1	1.47×10^{-5}	2.56	0.1535
Residual	4.01×10^{-5}	7	57313.48		
Lack of Fit	3.03×10^{-5}	3	1.01×10^{-5}	4.13	0.102
Pure Error	97,838.55	4	24,459.64		
Cor Total	9.88×10^{-6}	16			

showed promoting effects. However, because the value of A was larger (220-280) than the value of BC, the product terms of the heating rate and residence time had little effect on MY, which generally decreased with increasing temperature. For HHV, all three influencing factors, A, B, and C, had promoting effects, and only BC and B^2 showed a slight inhibitory effect. Therefore, temperature was the most important factor influencing HHV and MY.

Fig. 2 shows the residual diagram of MY and HHV. The experimental values are close to the theoretical data, indicating that the MY and HHV models are suitable for fitting the relationship between the three influencing factors (temperature, residence time, and heating rate) and the response value (MY and HHV) of the torrefaction process. This fitting relationship can also be expressed by the correlation coefficient (R^2). The R^2 value is in the range of 0-1, and the fitting effect is better when the value is close to 1. The correlation coefficients of MY and HHV were 0.9759 and 0.9594, respectively, indicating that there was a good correlation between the influencing factors and the response values. This phenomenon is consistent with that observed during Singh's research [25].

The F-value, p-value, lack of fit, and other data shown in Table 4 represent the accuracy of the model. Among them, F- and p-values are the most common standards used for this purpose. A model with the largest F-value and a p-value less than 0.05 can be considered reliable. The MY model had an F-value of 31.49 and a p-value <0.0001. For HHV, the F-value was 18.38 and the p-value was 0.0004; therefore, both models were deemed accurate. The F- and p-values can also be used to predict the influence of model factors, including those of linear terms (A, B, C), interaction terms

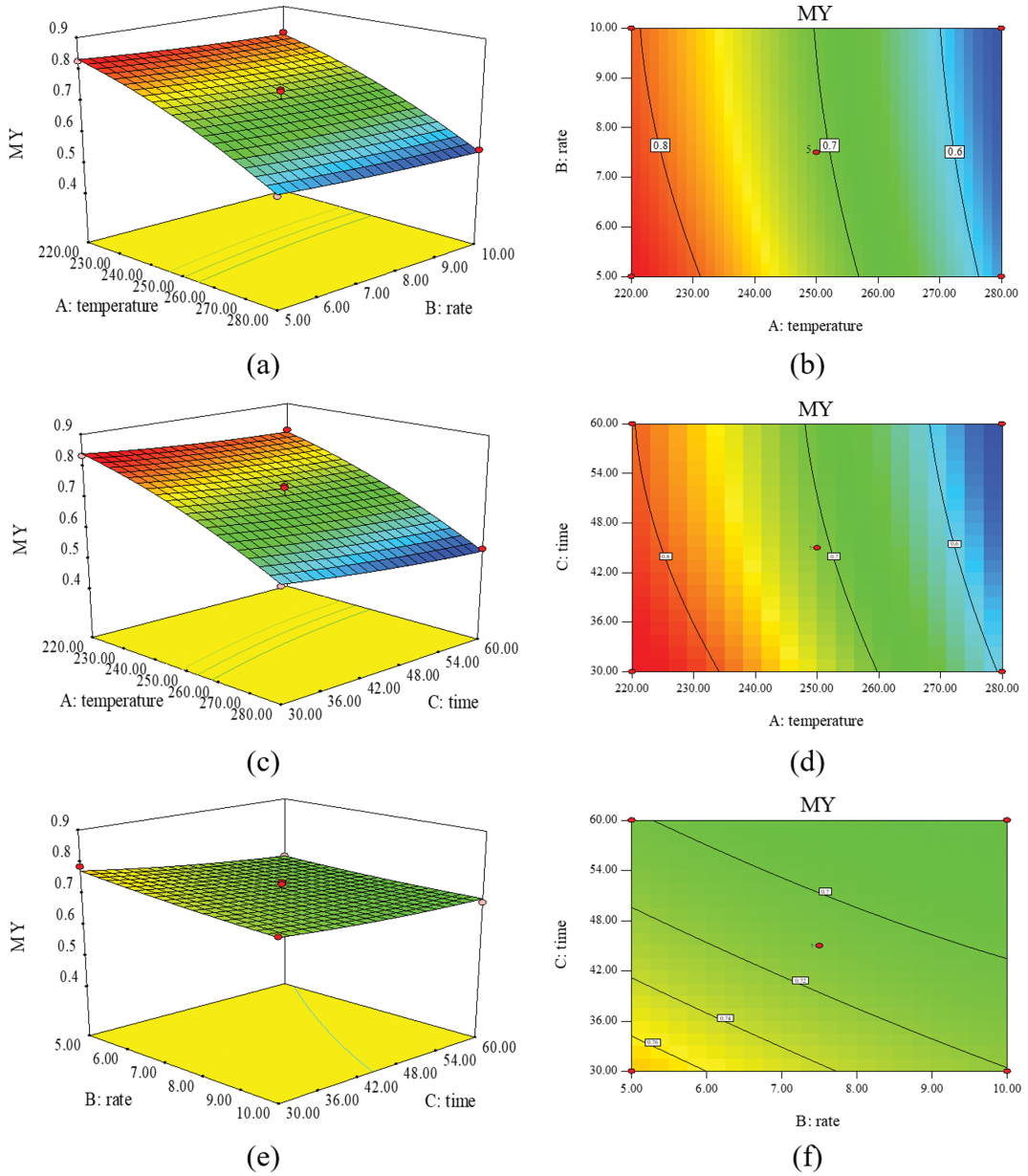

Fig. 3. Three-dimensional response surface and contour plots of MY showing the effect of temperature (°C), heating rate (°C/min), and residence time (min).

(AB, AC, BC), and quadratic terms (A^2, B^2, C^2). For MY, the values of A, B, C, and A^2 were 262.15, 4.05, 10.4, and 5.14, and for HHV, they were 130.51, 6.26, 4.22, and 6.96, respectively. Therefore, temperature and residence time were the main factors influencing MY. For HHV, because A^2 was greater than B and C, temperature was the most important factor affecting it. Except for temperature, other factors had similar effects on HHV. Peng et al. [48] reported similar conclusions for the torrefaction of different types of wood.

2-2. Parameter Interaction Analysis

Fig. 3(a), (b) shows the change in MY with the temperature and heating rate for a constant residence time of 45 min. As the temperature and heating rate increased, the MY continued to decrease. This can be explained by the fact that a higher heating rate inhibits the coking reaction and increases the tar production. Three-dimensional (3D) plots and contour plots of MY according to temperature and residence time are shown in Fig. 3(c), (d). At a heating rate of 7.5°C/min, the average range of MY decreased with an increasing temperature or residence time. A similar trend was observed for a fixed residence time. Fig. 3(e), (f) shows the effect of the heating rate and residence time on MY at 250°C. The 3D plot tended to form a plane, which indicates that MY is more susceptible to temperature than to heating rate and residence time. Accord-

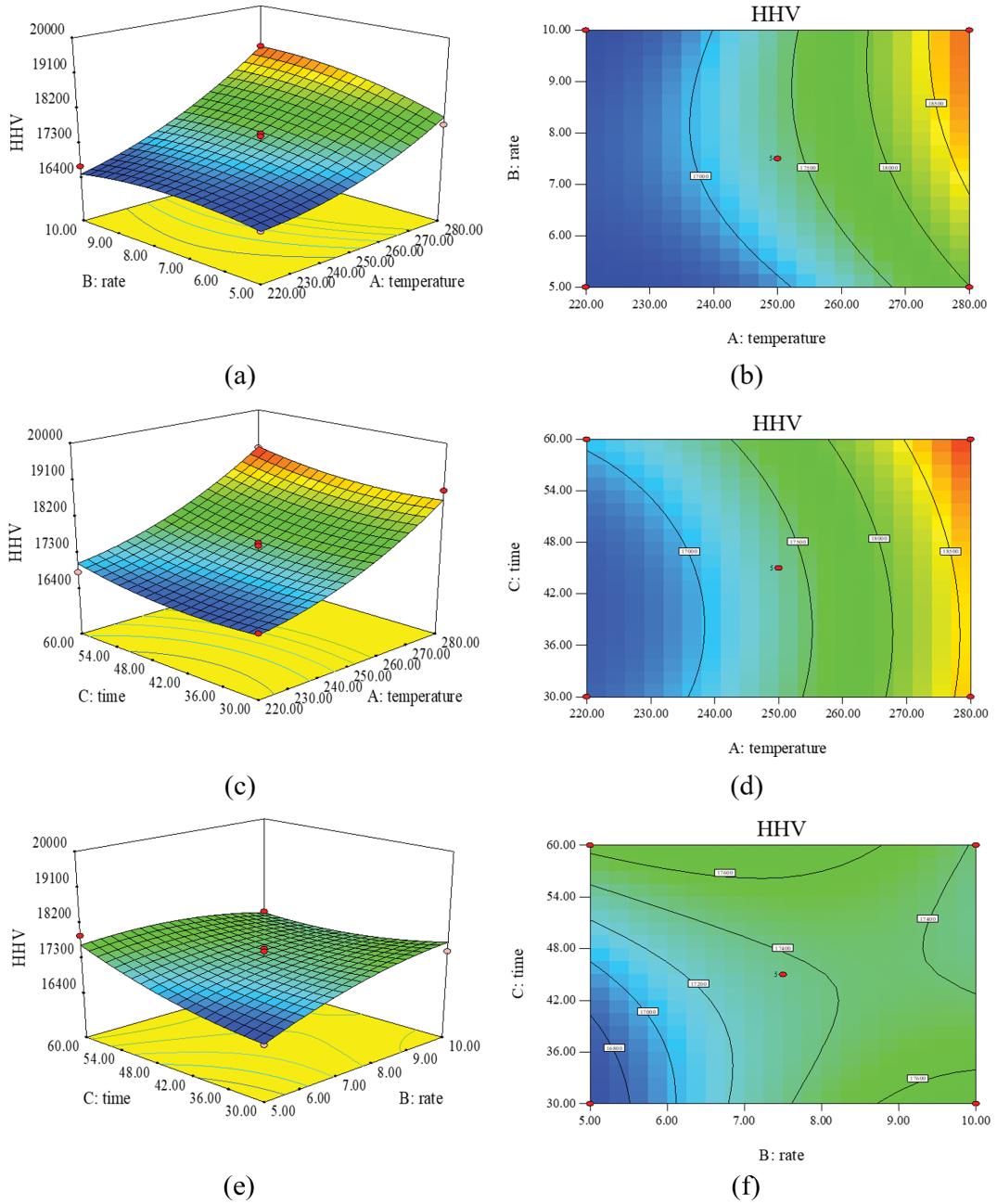

Fig. 4. Three-dimensional response surface and contour plots of HHV showing the effect of temperature (°C), heating rate (°C/min), and residence time (min).

Table 5. Optimized values of independent variables and responses

No.	Temperature (°C)	Heating rate (°C/min)	Residence time (min)	MY (%)	HHV (kJ/kg)	Desirability
1	242.26	6.28	60	72.45	17,696.8	0.551
2	242.3	6.25	60	72.44	17,697.2	0.551
3	242.08	6.3	60	72.51	17,692.7	0.551
4	242.03	6.27	60	72.55	17,690.2	0.551
5	243.1	6.28	60	72.10	17,718.8	0.551
6	241.94	6.12	60	72.66	17,682.2	0.551

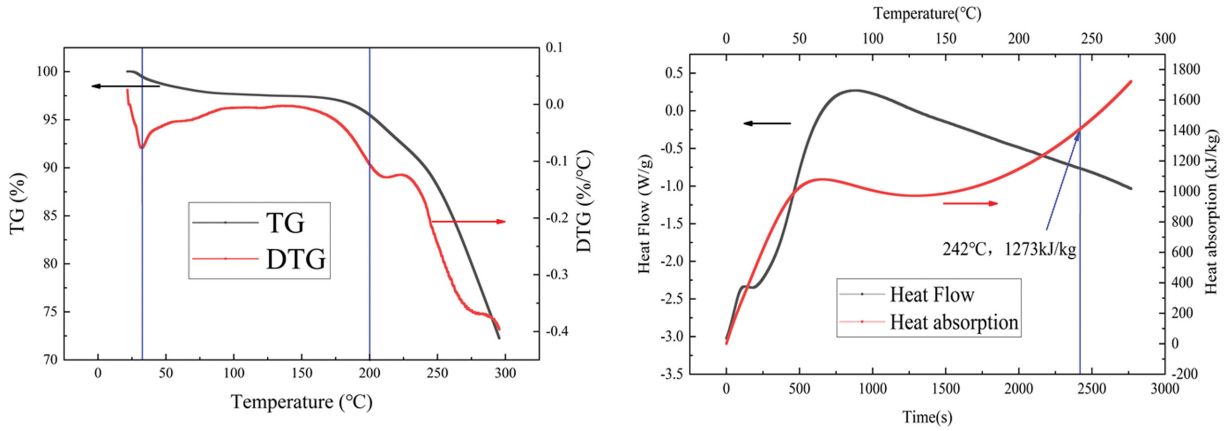

(a) TG-DTG (b) DSC

Fig. 5. TG-DTG and DSC of corn straw torrefaction at 6.28 °C/min heating rate and 60 min residence time.

ing to the F-values (B=4.05, C=10.4) shown in Table 2, the influence of residence time on MY was slightly greater than that of the heating rate. Similarly, regarding the p-value, B was 0.084, which is greater than 0.05, making it more untrustworthy.

Fig. 4(a), (b) and 4(c), (d) show the 3D and contour plots of HHV with other variables with a constant residence time (45 min) and heating rate (7.5°C/min), respectively. The general trend was the same as that for MY; the HHV increased as the independent variable increased. This increase in HHV occurred because as the temperature increased, the decomposition of the three components of corn straw also increased, and the decarbonylation, decarboxylation, and decomposition reactions of corn straw reduced the H/C and O/C ratios of the solid product [49]. Fig. 4(e), (f) shows the response plots of HHV with the residence time and heating rate. For a heating rate less than 8°C/min and residence time less than 48 min, HHV shows a slight increasing trend as the heating rate and time increase. After the heating rate and residence time increase considerably, the HHV remains nearly stable, and the 3D image is still close to a plane. Neither the heating rate nor the residence time significantly influence the HHV change in this phase. As shown in Table 4, the F-value of the heating rate (6.26) is greater than that of the residence time (4.22), and the p-value of the heating rate (0.0408) is within the allowable error range, whereas that of the residence time (0.079) is higher than 0.05. Therefore, the effect of the heating rate on HHV is greater than that of the residence time, but the effect of the heating rate on MY is weaker than that of the residence time.

2-3. Optimization of MY and HHV

One of the goals of this study was to define the energy balance of the torrefaction process. To improve the quality and yield of biochar, we used the Design-Expert program and set the maximum values of MY and HHV as optimization conditions, and the optimization results are shown in Table 5. The optimal conditions for the experiments were set to 242.26 °C, a residence time of 60 min, and heating rate of 6.28 °C/min. Because of instrument limitations, the room temperature was raised to 242 °C within 38 min when setting the temperature program. At this time, the heating rate was 6.37 °C/min. The measured MY and HHV were 0.7385 and 17,042.6 kJ/kg, respectively, with an error of less than 5% compared to the predicted values. Therefore, the predicted and experimental results were consistent.

3. Energy Balance of the Torrefaction Process

3-1. Endothermic Analysis of Torrefaction

TG-DSC was used to conduct torrefaction experiments of corn straw at a heating rate of 6.28 °C/min, and the heat absorption at different temperatures was analyzed. The TG-derivative thermogravimetry (DTG) and DSC curves are shown in Fig. 5.

Fig. 5(a) shows that at temperatures lower than 200 °C, the mass loss was small. Most of this mass loss occurred because of the dehydration reaction. At temperatures higher than 200 °C, hemicellulose began to decompose, and the mass loss started to increase; and as the temperature increased, the overall weight loss rate gradually increased [50]. Fig. 5(b) shows the DSC curve of corn straw heating at 6.28 °C/min up to 300 °C. At 300 °C, because of the de-

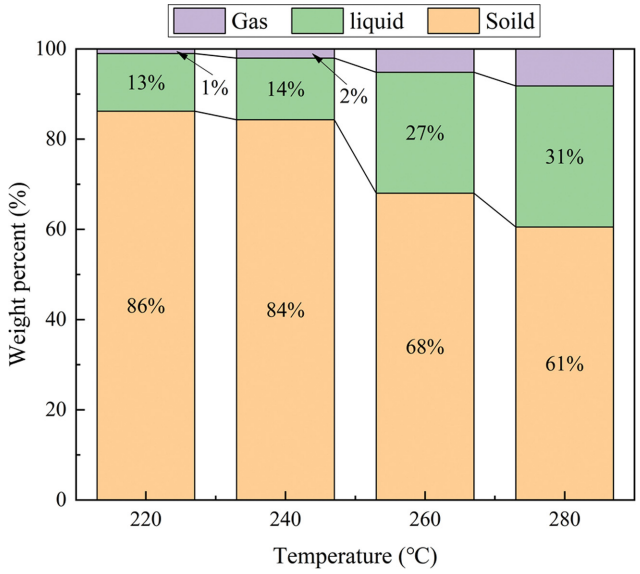

Fig. 6. Yield distribution of solid, liquid, and gas products at different temperatures.

composition of hemicellulose and the depolymerization and volatilization of cellulose, the DSC curve absorbed heat at the constant temperature stage. The amount of heat adsorption remained approximately the same, and even an exothermic phenomenon occurred at certain temperatures [51]. Therefore, this curve was only intercepted until the end of the heating phase to calculate the heat absorption of the torrefaction process. In the heating process, the heat absorption of the samples first increased, slowly decreased, and then increased again. Before 100 °C, the heat absorption tended to increase because the water contained in the corn straw absorbed heat. The subsequent decrease in heat absorption occurred because the initial hemicellulose decomposition that occurred was an exothermic reaction. As the temperature increased further, cellulose, hemicellulose, and lignin began to absorb heat. The data analysis indicated that at 242 °C, the thermal desorption heat was 1,273 kJ/kg, and at 300 °C, the heat absorption was 1,721 kJ/kg.

3-2. Heat Production During Torrefaction

Fig. 6 shows the solid, liquid, and gas yields of corn straw at 220, 240, 260, and 280 °C with the optimized heating rate and residence time. As the torrefaction products were divided into condensable gas and non-condensable gas, the tar and gas were calculated separately.

Fig. 6 shows that as the temperature increased, the solid yield continued to decrease, and the proportion of liquid and gas gradually increased. At temperatures lower than 240 °C, the gas yield was only 1-2%. This was the initial stage of torrefaction, at which only a small amount of hemicellulose was decomposed. As the temperature increased to 260 °C, cellulose and lignin began to decompose, and the mass loss increased. At 300 °C, the hemicellulose was mostly decomposed, and the distribution of the three terms (cellulose, hemicellulose and lignin) tended to be stable.

The tar components were analyzed by GC-MS based on the optimized heating rate (6.28 °C/min) and residence time (60 min), with corn straw torrefaction at 220, 240, 260, and 280 °C. Gallego et al. [52] observed that the HHV of tar is mainly composed of molecules with fewer than eight C atoms. Therefore, we selected data for molecules with fewer than eight C atoms at different temperatures for analysis and calculated the HHV of tar at different temperatures. The results of tar data and selected data are shown in Tables S1 and S2.

Table S2 shows the main components and HHV of tar at different temperatures. The HHV of tar did not change with temperature and was maintained at approximately 20 MJ/kg. Chen et al. [17] obtained a calorific value of 22.4 MJ/kg for tar in a study on bamboo torrefaction. Moreover, among the tar components at different temperatures, acetic acid presented the largest HHV. In addition to acetic acid, the main components of tar included alcohols, ketones, phenols, aldehydes, and esters. At lower temperatures, there were more acid products, and as the temperature increased, the amount of alcohol products gradually increased.

The composition results indicated that the number of main components increased with increasing temperature. This could be attributed to the catalytic cracking and decomposition of macromolecular compounds in the corn straw caused by the increase in temperature, which enhanced the production small molecular weight compounds with relatively fewer C atoms. By multiplying the HHV of tar at different temperatures (Table 6) by the proportion of condensable gas at that temperature, we obtained the heat of combustion of tar at different temperatures. The calculation results are shown in Table 6.

Table 6 shows that the heat of combustion of the liquid component increased rapidly at 240-260 °C, from 2,405.354 to 5,205.816 kJ/kg, which represents an increase of 116.4%. Until 280 °C, the heat of combustion further increased by 815.513 kJ/kg. According to Table 1, at 280 °C, MY was significantly low, which did not meet the research goal of obtaining the highest calorific value with minimal mass loss. Therefore, the energy balance was established at 240-260 °C in an attempt to meet the requirements of this study. MS was used to analyze the gas products (H_2, CO, CO_2, CH_4) at different temperatures, and their compositions and contents are shown in Fig. 7.

Fig. 7 shows that for all groups of experiments, the initial value

Table 6. Combustion heat of tar at different temperatures

Temperature (°C)	HHV (MJ/kg)	Tar (%)	Combustion heat (kJ/kg)
220	21.1815	13	2,753.595
240	17.1811	14	2,405.354
260	19.2808	27	5,205.816
280	19.4559	31	6,031.329

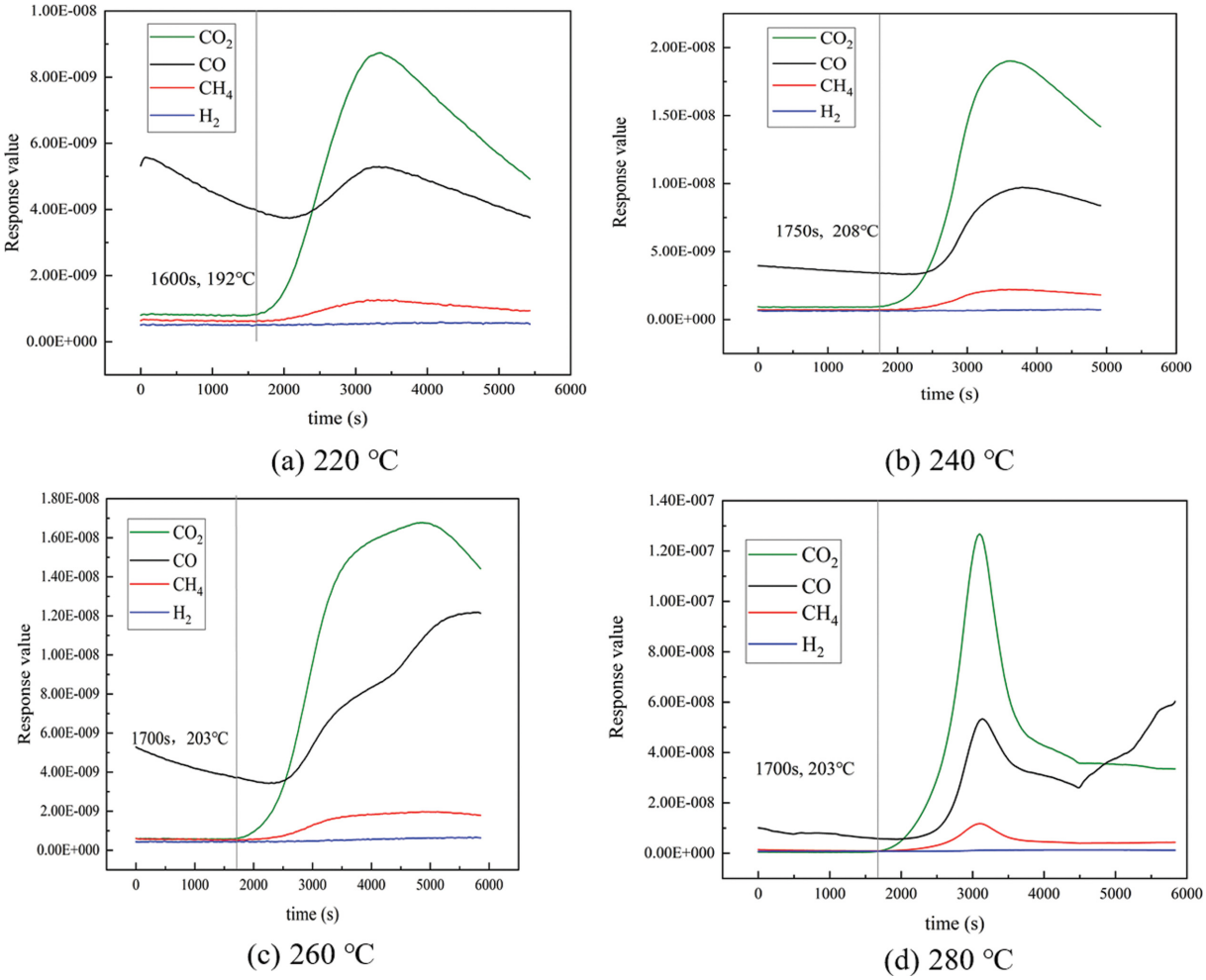

Fig. 7. Response values of gas components at different temperatures.

of CO was higher than that of the other three gases. This might be attributed to the mass-to-charge ratio of CO (=28) and air mass-to-charge ratio (=27), observed by MS, which indicate that air leakage might have caused this phenomenon. In the heating stage (reaction time less than 2,000 s), CO_2, CH_4, and H_2 presented no clear increasing trend, and only CO showed a decreasing trend. This phenomenon might have occurred because of the gas thermal expansion; specifically, when the temperature increased, the volume of argon increased, resulting in an increase in the gas flow rate in the device, and the amount of air leaking into the device decreased, which increased the relative content of argon. Moreover, the viscosity of tar at low temperatures is large and, thus, the phenomenon could also be explained by the secondary cracking reaction of tar as the temperature rises and the number of small molecules produced by macromolecular substances. Based on Eq. (3), the gas HHVs at different temperatures were calculated and are shown in Table 7.

Table 7. HHV of gas at different temperatures

Temperature (°C)	220	240	260	280
HHV_g (kJ/kg)	92.836	154.503	394.903	597.027

3-3. Energy Balance Analysis and Design of Bench-scale Torrefaction Equipment

Comparing the results shown in Fig. 4 and Tables 6 and 7, one could conclude that at 220-280 °C, if the total energy of the gas and liquid by-products was used to provide heat for the torrefaction process, the process would be fully self-sufficient. However, considering the incomplete fuel combustion and the heat loss during the energy transfer, we conservatively estimated wastage of approximately 50% of the energy. Therefore, 50% of the energy of the by-products was selected for establishing the energy balance based on Fig. 6. At 242 °C, the heat required for torrefaction was 1,273 kJ/kg, and at 240 °C, the heat loss was 50% and the by-product calorific value was 1,279.929 kJ/kg, which is almost at the critical point of torrefaction according to the energy balance. As the temperature increased, the calorific value of the by-products became higher than the energy required for torrefaction. Therefore, it was feasible to establish an energy balance based on the optimization conditions of the response surface method. According to the established energy balance, the bench-scale torrefaction experimental device was designed. The specific scheme is shown in Fig. 8.

The reactor was designed based on a capacity of 1-5 kg/h. To enhance the heat transfer efficiency, the device uses a combination

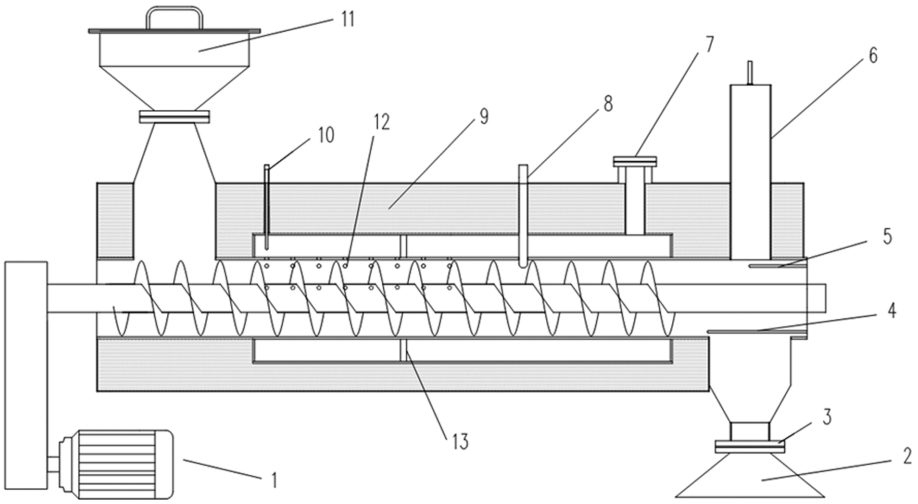

Fig. 8. Screw reactor for corn straw torrefaction.

1. Speed controller
2. Carbon collection
3. Gate
4, 5, 10. Thermocouple
6. Vent
7. Nitrogen inlet
8. Oxygen inlet
9. Insulation layer
11. Feen bin
12. Uniform flow orifice
13. Formwork-support

of internal and external heat to torrefy the corn straw. The inner tube of the screw reactor has a uniform flow orifice on the side of the feed bin. The high-temperature nitrogen which carried the heat replaces the heat generated by the combustion of the gas and liquid products of the torrefaction entering the reactor from the inlet, after filling the outer sleeve. The hot carrier gas enters the inner tube through the uniform flow orifice and torrefies the corn straw through heat conduction, convection heat transfer, and a small amount of radiant heat exchange. To ensure that the gas does not escape from the inlet and the outlet during the experiment, high-temperature gate valves were installed at the inlet and outlet. Thermocouples were installed at the uniform flow orifice, gas outlet, and solid outlet to measure the temperature so that the nitrogen temperature and flow rate could be adjusted according to the temperature indicated by the thermocouple (thermocouple 4, in Fig. 8). A processing capacity of 5 kg/h was set according to the data shown in Tables 6 and 7, such that the required processing capacity of the heater was 7.2 m^3/h and the power was 12 KW.

CONCLUSIONS

RSM was used to design a corn straw torrefaction experiment based on three influencing factors: temperature, heating rate, and residence time. MY and HHV were optimized, and the energy balance under optimal conditions was explored. The main conclusions are as follows:

1. At 242.26 °C, a 60 min residence time, and 6.28 °C/min heating rate, MY and HHV had maximum values at 0.7385 and 17,042.6 kJ/kg, respectively. The errors between the experimental and optimized results were within 5%. For MY, temperature was the most important factor affecting the degree of torrefaction, followed by residence time and then heating rate. For HHV, their magnitude of influence was in the following order: temperature>heating rate> residence time.

2. At 242 and 300 °C, the heat absorption was 1,273 and 1,721 kJ/kg, respectively. For a 50% energy loss, the HHV of the gas-liquid product of corn straw torrefaction at 240 °C was 1,279.929 kJ/kg, which just meets the demand of the energy balance, such that the energy balance was established above this temperature.

3. According to the established energy balance, a bench-scale experimental device for corn straw torrefaction was designed. The device can torrefy 5 kg of corn straw per hour, and the power and required processing capacity of the heater was 12 KW and 7.2 m^3/h, respectively. A bench-scale study on the torrefaction of corn straw provided the data variation for fluid-bed and bench-scale reactors and theoretical support for the construction of medium-sized and even industrialized experimental platforms.

ACKNOWLEDGEMENTS

We gratefully acknowledge the financial support provided by the National Natural Science Funds for Young Scholars of China (No. 51806033) and Jilin Provincial Science and Technology Development Program (No. 20190201096JC; No. 20190303025SF).

SUPPORTING INFORMATION

Additional information as noted in the text. This information is available via the Internet at http://www.springer.com/chemistry/journal/11814.

REFERENCES

1. F. Manzano-Agugliaro, A. Alcayde, F. G. Montoya, A. Zapata-Sierra and C. Gil, *Energy Rev.*, **18**, 134 (2013).
2. H. H. Bui, K.-Q. Tran and W. H. Chen, *Bioresour. Technol.*, **199**, 362 (2016).
3. A. Trubetskaya, J. J. Leahy, E. Yazhenskikh, M. Müller, P. Layden,

R. Johnson, K. Ståhl and R. F. D. Monaghan, *Energy* (Oxford), **171**, 853 (2019).
4. J. Wannapeera and N. Worasuwannarak, *J. Anal. Appl. Pyrolysis*, **96**, 173 (2012).
5. H. Moayedi, B. Aghel, M. M. Abdullahi, H. Nguyen and A. Rashid, *J. Cleaner Production*, **237**, 117851 (2019).
6. R. A. Sheldon, *Green Chem*., **16**, 95 (2014).
7. S. N. Naik, V. V. Goud, P. K. Rout and A. K. Dalai, *Renew. Sustain. Energy Rev*., **14**, 578 (2010).
8. J. Park, J. Meng, K. H. Lim, O. J. Rojas and S. Park, *J. Anal. Appl. Pyrolysis*, **100**, 199 (2013).
9. S. N. Naik, V. V Goud, P. K. Rout and A. K. Dalai, *Renew. Sustain. Energy Rev*., **14**, 578 (2010).
10. J. Deng, G. Wang, J. Kuang, Y. Zhang and Y. Luo, *J. Anal. Appl. Pyrolysis*, **86**, 331 (2009).
11. P. Basu, A. K. Sadhukhan, P. Gupta, S. Rao, A. Dhungana and B. Acharya, *Bioresour. Technol*., **159**, 215 (2014).
12. K. Q. Tran, X. Luo, G. Seisenbaeva and R. Jirjis, *Appl. Energy*, **112**, 539 (2013).
13. W. H. Chen, K. M. Lu and C. M. Tsai, *Appl. Energy*, **100**, 318 (2012).
14. W. H. Chen, H. C. Hsu, K. M. Lu, W. J. Lee and T. C. Lin, *Energy*, **36**, 3012 (2011).
15. L. J. R. Nunes, J. C. O. Matias and J. P. S. Catalão, *Energy Rev*., **40**, 153 (2014).
16. W. H. Chen and P. C. Kuo, *Energy* (Oxford), **36**, 803 (2011).
17. W. H. Chen, S. H. Liu, T. T. Juang, C. M. Tsai and Y. Q. Zhuang, *Appl. Energy*, **160**, 829 (2015).
18. H. Pawlak-Kruczek, K. Krochmalny, K. Mościcki, J. Zgóra, M. Czerep, M. Ostrycharczyk and Ł Niedźwiecki, *Inżynieria i ochrona środowiska*, **20**, 457 (2017).
19. M. H. Sulaiman, Y. Uemura and M. T. Azizan, *Procedia Eng*., **148**, 573 (2016).
20. B. S. Chiou, D. Valenzuela-Medina, C. Bilbao-Sainz, A. K. Klamczynski, R. J. Avena-Bustillos, R. R. Milczarek, W. X. Du, G. M. Glenn and W. J. Orts, *Bioresour. Technol*., **177**, 58 (2015).
21. H. Li, X. Liu, R. Legros, X. T. Bi, C. Jim Lim and S. Sokhansanj, *Appl. Energy*, **93**, 680 (2012).
22. Y. Liu, E. Rokni, R. Yang, X. Ren, R. Sun and Y. A. Levendis, *Fuel*, **285**, 119044 (2021).
23. S. Zhang, Y. Su, Y. Xiong and H. Zhang, *Fuel*, **262**, 116667 (2020).
24. O. Kutlu and G. Kocar, *Int. J. Energy Res*., **42**, 4746 (2018).
25. S. Singh, J. P. Chakraborty and M. K. Mondal, *Energy* (Oxford), **186**, 115865 (2019).
26. D. A. Granados, H. I. Velásquez and F. Chejne, *Energy* (Oxford), **74**, 181 (2014).
27. R. B. Bates and A. F. Ghoniem, *Bioresour. Technol*., **134**, 331 (2013).
28. R. A. Dos Reis Ferreira, C. Da Silva Meireles, R. M. N. Assunção and R. Reis Soares, *J. Therm. Anal. Calorim*., **132**, 1535 (2018).
29. R. K. Singh, K. Jena, J. P. Chakraborty and A. Sarkar, *Int. J. Hydrogen Energy*, **45**, 18922 (2020).
30. A. Ohliger, M. Förster and R. Kneer, *Fuel*, **104**, 607 (2013).
31. D. Medic, M. Darr, A. Shah, B. Potter and J. Zimmerman, *Fuel*, **91**, 147 (2012).
32. P. Bergman and A. R. Boersma (2005) [https://www.researchgate.net/publication/204978559].
33. M. Mohadesi, B. Aghel, M. Maleki and A. Ansari, *Fuel*, **273**, 117736 (2020).
34. B. Aghel, M. Mohadesi and S. Sahraei, *Chem. Eng. Technol*., **41**, 598 (2018).
35. B. Aghel, M. Mohadesi, A. Ansari and M. Maleki, *Renewable Energy*, **142**, 207 (2019).
36. L. E. Arteaga-Pérez, C. Segura, V. Bustamante-García, O. Cápiro and R. Jiménez, *Energy* (Oxford), **93**, 1731 (2015).
37. S. Chang, Z. Zhao, A. Zheng, F. He, Z. Huang and H. Li, *Energy Fuels*, **26**, 7009 (2012).
38. L. E. Arteaga-Pérez, H. Grandón, M. Flores, C. Segura and S. S. Kelley, *Bioresour. Technol*., **238**, 194 (2017).
39. G. J. Wang, Y. H. Luo, D. Jian, J. H. Kuang and Y. L. Zhang, *Chinese Sci. Bull*., **56**, 1442 (2011).
40. P. T. Williams and N. Nugranad, *Energy*, **25**, 493 (2000).
41. M. Irfan, Q. Chen, Y. Yue, R. Pang, Q. Lin, X. Zhao and H. Chen, *Bioresour. Technol*., **211**, 457 (2016).
42. J. Wannapeera, B. Fungtammasan and N. Worasuwannarak, *J. Anal. Appl. Pyrolysis*, **92**, 99 (2011).
43. B. M. Esteves and H. M. Pereira, *Bioresources*, **4**, 370 (2009).
44. B. Esteves, A. V. Marques, I. Domingos and H. Pereira, *Wood Sci. Technol*., **42**, 369 (2008).
45. M. M. Gonzalez-Pena and M. Hale, *Holzforschung*, **63**, 385 (2009).
46. T. Melkior, C. Barthomeuf and M. Bardet, *Fuel*, **187**, 250 (2017).
47. M. R. Pelaez-Samaniego, V. Yadama, E. Lowell and R. Espinoza-Herrera, *Wood Sci. Technol*., **47**, 1285 (2013).
48. J. H. Peng, X. T. Bi, S. Sokhansanj and C. J. Lim, *Fuel*, **111**, 411 (2013).
49. C. M. S. Da Silva, A. D. C. O. Carneiro, B. R. Vital, C. G. Figueiró, L. D. F. Fialho, M. A. de Magalhães, A. G. Carvalho and W. L. Candido, *Renew. Sustain. Energy Rev*., **82**, 2426 (2018).
50. J. Ribeiro, R. Godina, J. Matias and L. Nunes, *Sustain* (Basel, Switzerland), **10**, 2323 (2018).
51. I. Milosavljevic, V. Oja and E. M. Suuberg, *Ind. Eng. Chem. Res*., **35**, 653 (1996).
52. L. J. Gallego, S. Cardona, E. Martínez and L. A. Rios, *Waste and Biomass Valorization*, **11**, 2273 (2020).

Supporting Information

Response surface analysis of energy balance and optimum condition for torrefaction of corn straw

Shuai Guo, Tiankuo Guo, Deyong Che, Hongpeng Liu, and Baizhong Sun†

School of Energy and Power Engineering, Northeast Electric Power University, Jilin 132012, China
(*Received 14 August 2021 • Revised 4 November 2021 • Accepted 29 November 2021*)

The tar composition and content are measured by GC-MS, and the data obtained is sorted in the Table S1.

Table S1. Composition of tar at different temperatures

220 °C						
No	RT	COMPOUND	MF	FORMULOR	CAS	AREA
1	3.1777	Cyclotetrasiloxane, octamethyl-	66.2	C8H24O4Si4	556-67-2	118,138.8
2	4.4093	2,3-Pentanedione	54.9	C5H8O2	600-14-6	48,047.5
3	6.4379	Pyridine	54.4	C5H5N	110-86-1	45,286.9
4	8.066	Diethyl(3-decyn-1-yl)amine	63.5	C14H27N	63791-57-1	132,077.8
5	8.7113	2-Propanone, 1-hydroxy-	60.7	C3H6O2	116-09-6	727221.9
6	9.2862	2-Pentanone, 4-hydroxy-4-methyl-	77.6	C6H12O2	123-42-2	151,249
7	10.4362	Acetic acid	86	C2H4O2	64-19-7	2,466,554.8
8	10.5881	2-Propanone, 1-(acetyloxy)-	64.3	C5H8O3	592-20-1	160,773.1
9	10.6294	3-Furaldehyde	84	C5H4O2	498-60-2	1,906,673.5
10	11.5293	Propanoic acid	54.3	C3H6O2	1979/9/4	42,807.9
11	11.8994	2-Furancarboxaldehyde, 5-methyl-	81.5	C6H6O2	620-02-0	196,976.6
12	12.0661	4-Cyclopentene-1,3-dione	50.1	C5H4O2	930-60-9	31,792.7
13	12.3239	Cyclooctasiloxane, hexadecamethyl-	65.1	C16H48O8Si8	556-68-3	6,983
14	13.1995	Methylenecyclopropanecarboxylic acid	73.9	C5H6O2	62266-36-8	168,399.9
15	13.7908	Cyclononasiloxane, octadecamethyl-	51.3	C18H54O9Si9	556-71-8	7,580.5
16	13.9026	Benzenol, 4-n-propyloxy-O-[4-[1-cycloazapropyl]-n-butyl]-	58.4	C15H23NO2	23618-02-2	48,714.1
17	14.7555	Phenol, 2-methoxy-	76.8	C7H8O2	1990/5/1	117,193.9
18	15.0966	Cyclodecasiloxane, eicosamethyl-	64.9	C20H60O10Si10	18772-36-6	25,526.4
19	16.0235	Phenol	61.7	C6H6O	108-95-2	477,349.7
20	16.3097	Cyclodecasiloxane, eicosamethyl-	63.5	C20H60O10Si10	18772-36-6	24,304.5
21	16.9807	Acetic acid, [(aminocarbonyl)amino]oxo-	55.2	C3H4N2O4	585-05-7	87,527.7
22	17.4034	(2S,6R,7S,8E)-(+)-2,7-Epoxy-4,8-megastigmadiene	57.9	C13H20O	108342-25-2	44,993.2
23	17.4527	Cyclononasiloxane, octadecamethyl-	50.2	C18H54O9Si9	556-71-8	51,460.4
24	17.5418	5-Acetoxymethyl-2-furaldehyde	73	C8H8O4	10551-58-3	156,780.8
25	17.5816	Phenol, 5-ethenyl-2-methoxy-	81.7	C9H10O2	621-58-9	361,664.2
26	18.0896	Phenol, 2,6-dimethoxy-	71.5	C8H10O3	1991/10/1	96,234.3
27	18.5161	Cyclodecasiloxane, eicosamethyl-	51.1	C20H60O10Si10	18772-36-6	16,470.9
28	19.0489	N-Benzyl-2-phenethylamine	75.2	C15H17N	3647-71-0	1,533,023.2
29	19.5229	Cyclodecasiloxane, eicosamethyl-	71.7	C20H60O10Si10	18772-36-6	12,711.5
30	20.3211	5-Hydroxymethylfurfural	70.1	C6H6O3	67-47-0	457,592.3

Table S1. Continued

240 °C						
No	RT	COMPOUND	MF	FORMULOR	CAS	AREA
1	3.2045	Cyclotetrasiloxane, octamethyl-	76	C8H24O4Si4	556-67-2	5,819,346.6
2	4.4243	2,3-Pentanedione	67.9	C5H8O2	600-14-6	69,506.7
3	5.9591	Cyclopentasiloxane, decamethyl-	74.6	C10H30O5Si5	541-02-6	433,286.9
4	6.6659	4,6′-Dimethoxy-2'-(tert.-butyldimethylsilyl)oxychalcone	57.6	C23H30O4Si	1000454-23-8	48,198.9
5	8.0776	N,N-Diethylheptylamine	71.8	C11H25N	1000391-35-1	189,772.6
6	8.3846	Acetoin	51.2	C4H8O2	513-86-0	38,366.9
7	8.5911	Cyclohexasiloxane, dodecamethyl-	70.6	C12H36O6Si6	540-97-6	185,748.7
8	8.7162	2-Propanone, 1-hydroxy-	73.7	C3H6O2	116-09-6	1,619,512.3
9	9.2998	2-Pentanone, 4-hydroxy-4-methyl-	76	C6H12O2	123-42-2	144,904.8
10	9.5063	1,2-Ethanediol, monoacetate	56.8	C4H8O3	542-59-6	127,020.6
11	9.7735	Propanoic acid, anhydride	52.5	C6H10O3	123-62-6	158,204.6
12	10.2018	4-Methyl-2H-pyran	63.5	C6H8O	1000432-32-7	69,707.1
13	10.4254	Acetic acid	88.4	C2H4O2	64-19-7	4,055,121.3
14	10.596	2-Propanone, 1-(acetyloxy)-	75.9	C5H8O3	592-20-1	324,070.5
15	10.6358	3-Furaldehyde	68.4	C5H4O2	498-60-2	2,304,317.4
16	11.1266	1-Pentanone, 1-(2-furanyl)-	63.6	C9H12O2	3194-17-0	58,035.9
17	11.5132	Propanoic acid	64.8	C3H6O2	1979/9/4	136,839.5
18	11.9036	2-Furancarboxaldehyde, 5-methyl-	74.7	C6H6O2	620-02-0	249,297.5
19	12.0704	4-Cyclopentene-1,3-dione	55.6	C5H4O2	930-60-9	65,818.9
20	12.3281	Cyclooctasiloxane, hexadecamethyl-	66.6	C16H48O8Si8	556-68-3	151,583.6
21	13.1981	Methylenecyclopropanecarboxylic acid	69.5	C5H6O2	62266-36-8	355,921.8
22	13.7971	Cyclononasiloxane, octadecamethyl-	70.8	C18H54O9Si9	556-71-8	99,168.1
23	13.8995	2-Cyclopenten-1-one, 2-hydroxy-	71.7	C5H6O2	10493-98-8	263,047.4
24	14.4378	2-Cyclopenten-1-one, 2-hydroxy-3-methyl-	54.7	C6H8O2	80-71-7	72,596.5
25	14.7562	Phenol, 2-methoxy-	81.1	C7H8O2	1990/5/1	305,982
26	15.0955	Cyclodecasiloxane, eicosamethyl-	72.4	C20H60O10Si10	18772-36-6	86,789.7
27	16.0224	Phenol	77.9	C6H6O	108-95-2	865,571.4
28	16.2366	Phenol, 4-ethyl-2-methoxy-	68.3	C9H12O2	2785-89-9	71,873.4
29	16.3068	Cyclodecasiloxane, eicosamethyl-	65.4	C20H60O10Si10	18772-36-6	100,561.2
30	16.9797	Cyclobutanol	61.2	C4H8O	2919-23-5	256,960.8
31	17.4062	(2S,6R,7S,8E)-(+)-2,7-Epoxy-4,8-megastigmadiene	61.8	C13H20O	108342-25-2	78,690.6
32	17.4404	Cyclononasiloxane, octadecamethyl-	53	C18H54O9Si9	556-71-8	52,408.4
33	17.539	5-Acetoxymethyl-2-furaldehyde	66.5	C8H8O4	10551-58-3	136,274
34	17.5769	Phenol, 5-ethenyl-2-methoxy-	84.9	C9H10O2	621-58-9	839,294.8
35	18.0849	Phenol, 2,6-dimethoxy-	80.9	C8H10O3	1991/10/1	290,160.5
36	18.5114	Cyclodecasiloxane, eicosamethyl-	54.2	C20H60O10Si10	18772-36-6	90,520.3
37	18.7238	Phenol, 2-methoxy-4-(1-propenyl)-	57.4	C10H12O2	97-54-1	54,569.2
38	19.0461	N-Benzyl-2-phenethylamine	75.7	C15H17N	3647-71-0	2,460,270.1
39	19.5125	Cyclodecasiloxane, eicosamethyl-	55.5	C20H60O10Si10	18772-36-6	115,115.8
40	20.3145	5-Hydroxymethylfurfural	69.2	C6H6O3	67-47-0	654,840.9
41	21.0995	2-Propanone, 1-(4-hydroxy-3-methoxyphenyl)-	54	C10H12O3	2503-46-0	70,309.3
42	22.1897	Cyclodecasiloxane, eicosamethyl-	50.5	C20H60O10Si10	18772-36-6	49,538.9
43	28.7062	Bis(2-ethylhexyl) phthalate	61.7	C24H38O4	117-81-7	95,634.8

Table S1. Continued

260 °C						
No	RT	COMPOUND	MF	FORMULOR	CAS	AREA
1	3.1874	2,3-Butanedione	60.5	C4H6O2	431-03-8	583,366.5
2	4.4186	2,3-Pentanedione	77.7	C5H8O2	600-14-6	100,788.8
3	8.0791	Aniline, N-(2-(diethylamino)ethyl)-2,4-dinitro-	69.7	C12H18N4O4	56223-91-7	256,239.2
4	8.7081	2-Propanone, 1-hydroxy-	79.3	C3H6O2	116-09-6	3,796,056
5	9.2046	1,2,4,5-Tetrazine	74.1	C2H2N4	290-96-0	190,669.7
6	9.3012	2-Pentanone, 4-hydroxy-4-methyl-	82.1	C6H12O2	123-42-2	196,135.7
7	9.5058	1,2-Ethanediol, monoacetate	67.6	C4H8O3	542-59-6	194,186.7
8	9.7673	Propanoic acid, anhydride	57.8	C6H10O3	123-62-6	173,116.4
9	10.1993	4-Methyl-2H-pyran	72.1	C6H8O	1000432-32-7	185,004
10	10.2656	Mepivacaine	60.5	C15H22N2O	96-88-8	59901.3
11	10.4021	Acetic acid	89.4	C2H4O2	64-19-7	7,075,773.1
12	10.5404	4-Chloro-3-methyl-2-butenyl acetate	53.8	C7H11ClO2	1000433-28-3	248,460.2
13	10.5954	2-Propanone, 1-(acetyloxy)-	81.1	C5H8O3	592-20-1	664,349.5
14	10.6352	3-Furaldehyde	74.7	C5H4O2	498-60-2	4,365,395.6
15	10.7148	2-Butanone	52.3	C4H8O	78-93-3	43,648
16	11.124	1-Pentanone, 1-(2-furanyl)-	79	C9H12O2	3194-17-0	188,887.3
17	11.1582	Furan, 2-(dichloromethyl)-tetrahydro-	66	C5H8Cl2O	931-05-5	92,467.5
18	11.4954	Propanoic acid	82.1	C3H6O2	1979/9/4	323,749.8
19	11.9028	2-Furancarboxaldehyde, 5-methyl-	86.5	C6H6O2	620-02-0	499,608.4
20	12.3254	Cyclooctasiloxane, hexadecamethyl-	66.6	C16H48O8Si8	556-68-3	174,805.9
21	12.7272	Cyclopentanecarboxylic acid, 2-fluorophenyl ester	56.6	C12H13FO2	1000325-76-5	33,513.1
22	13.0683	2-Cyclopenten-1-one, 3-ethyl-2-hydroxy-	68.3	C7H10O2	21835-01-8	53,722.3
23	13.1917	Methylenecyclopropanecarboxylic acid	83.9	C5H6O2	62266-36-8	926,986.8
24	13.796	Cyclononasiloxane, octadecamethyl-	63.1	C18H54O9Si9	556-71-8	73,817
25	13.8926	2-Cyclopenten-1-one, 2-hydroxy-	87	C5H6O2	10493-98-8	677,689.4
26	14.4346	2-Cyclopenten-1-one, 2-hydroxy-3-methyl-	80.3	C6H8O2	80-71-7	275,477.3
27	14.7549	Phenol, 2-methoxy-	85.2	C7H8O2	1990/5/1	622,916.7
28	14.88	Oxazolidine, 2,2-diethyl-3-methyl-	63.8	C8H17NO	161500-43-2	142,130.5
29	15.0941	Cyclodecasiloxane, eicosamethyl-	71.2	C20H60O10Si10	18772-36-6	41,228.6
30	15.6097	2-Methoxy-5-methylphenol	75.2	C8H10O2	1195-09-1	68,530.7
31	16.0209	Phenol	81.2	C6H6O	108-95-2	1,522,312.3
32	16.2332	Phenol, 4-ethyl-2-methoxy-	77.5	C9H12O2	2785-89-9	180,193.4
33	16.309	Cyclodecasiloxane, eicosamethyl-	63.4	C20H60O10Si10	18772-36-6	30,441.9
34	16.9781	Pentanal	69.8	C5H10O	110-62-3	415,866
35	17.4027	(2S,6R,7S,8E)-(+)-2,7-Epoxy-4,8-megastigmadiene	77.7	C13H20O	108342-25-2	260,764.5
36	17.4482	Cyclononasiloxane, octadecamethyl-	55.7	C18H54O9Si9	556-71-8	32,448.6
37	17.5411	5-Acetoxymethyl-2-furaldehyde	72.1	C8H8O4	10551-58-3	178,162.5
38	17.5771	Phenol, 5-ethenyl-2-methoxy-	85.3	C9H10O2	621-58-9	1,177,031.6
39	18.0832	Phenol, 2,6-dimethoxy-	83.8	C8H10O3	1991/10/1	574,976.6
40	18.6841	3,5-Heptanedione, 2,2,6,6-tetramethyl-	55.1	C11H20O2	1118-71-4	22,195.1
41	18.7258	trans-Isoeugenol	63.2	C10H12O2	5932-68-3	107,382.2
42	19.0461	N-Benzyl-2-phenethylamine	75.9	C15H17N	3647-71-0	3,611,037.9
43	19.1201	5-tert-Butylpyrogallol	55.5	C10H14O3	20481-17-8	57,965.5
44	20.0472	1,2-Benzenedicarboxylic acid, bis(2-methylpropyl) ester	77.5	C16H22O4	84-69-5	789,521.9
45	20.3107	5-Hydroxymethylfurfural	71.9	C6H6O3	67-47-0	1,075,463.6
46	21.0975	Guaiacol, 4-butyl-	63.5	C11H16O2	59832-96-1	154,043.8
47	21.7516	Phenol,2,6-dimethoxy-4-(2-propenyl)-	72.8	C11H14O3	6627-88-9	140,794.2
48	25.6783	Syringylacetone	64.6	C11H14O4	19037-58-2	142,120.5

Table S1. Continued

280 °C						
No	RT	COMPOUND	MF	FORMULOR	CAS	AREA
1	3.1855	2,3-Butanedione	77.1	C4H6O2	431-03-8	578,464.1
2	4.1057	Benzyl isopentyl ether	75.4	C12H18O	122-73-6	106,494.2
3	4.4187	2,3-Pentanedione	78.7	C5H8O2	600-14-6	107,822.2
4	8.0779	Acetamide, 2-diethylamino-N-(4,5,6,7-tetrahydro-2-cyanobenzo[b]thiophen-3-yl)-	69.5	C15H21N3OS	1000260-12-1	184,756.6
5	8.3621	Acetoin	51.5	C4H8O2	513-86-0	2,263.5
6	8.705	2-Propanone, 1-hydroxy-	80.1	C3H6O2	116-09-6	3,647,054.3
7	9.2033	1,2,4,5-Tetrazine	76.4	C2H2N4	290-96-0	235,885.1
8	9.2981	2-Pentanone, 4-hydroxy-4-methyl-	82	C6H12O2	123-42-2	160,504.2
9	9.5046	Acetic acid, (acetyloxy)-	64.2	C4H6O4	13831-30-6	203,024.4
10	9.7756	Propanoic acid, anhydride	60.3	C6H10O3	123-62-6	264,506.4
11	10.1981	4-Methyl-2H-pyran	74.7	C6H8O	1000432-32-7	154,138.3
12	10.2625	2(3H)-Furanone, 5-methyl-	62.6	C5H6O2	591-12-8	38,008
13	10.4122	Acetic acid	90.3	C2H4O2	64-19-7	5,728,867.1
14	10.5392	Propanoic acid, 2-oxo-, methyl ester	50	C4H6O3	600-22-6	215,957.8
15	10.5941	2-Propanone, 1-(acetyloxy)-	80.9	C5H8O3	592-20-1	563,720.6
16	10.6358	3-Furaldehyde	81.6	C5H4O2	498-60-2	3,293,155.1
17	11.1228	1-Pentanone, 1-(2-furanyl)-	79.9	C9H12O2	3194-17-0	227,244.4
18	11.1588	Furan, 2-(dichloromethyl)-tetrahydro-	68.7	C5H8Cl2O	931-05-5	255,599.2
19	11.2782	2,3-dimethylfuran	65.9	C6H8O	1000458-49-9	51,465.4
20	11.4999	Propanoic acid	75.6	C3H6O2	1979/9/4	280,913.2
21	11.9035	2-Furancarboxaldehyde, 5-methyl-	86.7	C6H6O2	620-02-0	396,999.5
22	12.3298	Cyclooctasiloxane, hexadecamethyl-	79.2	C16H48O8Si8	556-68-3	60,003.3
23	12.5515	Butanoic acid, 4-hydroxy-	64.6	C4H8O3	591-81-1	62,646.4
24	12.7297	3-Hexen-2-one, 5-methyl-	61	C7H12O	5166-53-0	31,330.1
25	13.0461	Furan, 2-methoxy-	55.1	C5H6O2	25414-22-6	31,182.1
26	13.1939	Methylenecyclopropanecarboxylic acid	84.7	C5H6O2	62266-36-8	779,565.6
27	13.8003	Cyclononasiloxane, octadecamethyl-	64.9	C18H54O9Si9	556-71-8	188,704.4
28	13.8951	2-Cyclopenten-1-one, 2-hydroxy-	86.2	C5H6O2	10493-98-8	723,066.7
29	14.4333	2-Cyclopenten-1-one, 2-hydroxy-3-methyl-	81.5	C6H8O2	80-71-7	302,561.9
30	14.7536	Phenol, 2-methoxy-	85.7	C7H8O2	1990/5/1	561,450.1
31	14.8786	DL-Norleucine amide, N,N,N'N'-tetramethyl-	59.5	C10H22N2O	1000453-48-5	126,515.8
32	15.0303	2-Cyclopenten-1-one, 3-ethyl-2-hydroxy-	76.6	C7H10O2	21835-01-8	53,617.2
33	15.0928	Cyclodecasiloxane, eicosamethyl-	62	C20H60O10Si10	18772-36-6	15,675.6
34	15.6121	2-Methoxy-5-methylphenol	74.7	C8H10O2	1195-09-1	70,203.7
35	16.0203	Phenol	80.4	C6H6O	108-95-2	1,191,113.1
36	16.2337	Phenol, 4-ethyl-2-methoxy-	78.8	C9H12O2	2785-89-9	195,273.1
37	16.6545	Phenol, 3-ethyl-	69.2	C8H10O	620-17-7	33,696.4
38	16.9767	Cyclobutanol	67.2	C4H8O	2919-23-5	447,876.7
39	17.4013	(2S,6R,7S,8E)-(+)-2,7-Epoxy-4,8-megastigmadiene	74.7	C13H20O	108342-25-2	211,205.6
40	17.5378	5-Acetoxymethyl-2-furaldehyde	69.5	C8H8O4	10551-58-3	82,136.2
41	17.5776	Phenol, 5-ethenyl-2-methoxy-	85.9	C9H10O2	621-58-9	915,468.7
42	18.0836	Phenol, 2,6-dimethoxy-	81	C8H10O3	1991/10/1	530,943.8
43	18.1708	3-ACETYL-3-METHYL-.gamma.-BUTYROLACTONE	53.5	C7H10O3	1000426-87-3	34,662.1
44	18.3376	5H-Benzo[b]pyran-8-ol, 2,3,5,5,8a-pentamethyl-6,7,8,8a-tetrahydro-	56.6	C14H22O2	97306-66-6	6,324.2
45	18.7244	3-Allyl-6-methoxyphenol	62.8	C10H12O2	501-19-9	101,309
46	19.0447	N-Benzyl-2-phenethylamine	75.4	C15H17N	3647-71-0	2,323,715.8
47	19.1225	Benzene, 1,2,3-trimethoxy-5-methyl	59.5	C10H14O3	6443-69-2	50,328
48	19.4258	1,4:3,6-Dianhydro-.alpha.-d-glucopyranose	60.6	C6H8O4	1000098-14-8	108,724.4
49	20.0476	1,2-Benzenedicarboxylic acid, bis(2-methylpropyl) ester	78.2	C16H22O4	84-69-5	698,696.7
50	20.3074	5-Hydroxymethylfurfural	69.8	C6H6O3	67-47-0	682,381.9
51	21.0923	2-Propanone, 1-(4-hydroxy-3-methoxyphenyl)-	62.9	C10H12O3	2503-46-0	126,952.4
52	21.7483	Phenol,2,6-dimethoxy-4-(2-propenyl)-	70.9	C11H14O3	6627-88-9	171,053.6
53	25.6811	Syringylacetone	61.7	C11H14O4	19037-58-2	146,345.8

The data for molecules with less than eight C atoms at different temperatures for analysis and calculated the HHV of tar at different temperatures, the results are shown in Table S2.

Table S2. Composition and HHV (MJ/kg) of tar at different temperatures

	220 °C		240 °C	
No	Component	HHV	Component	HHV
1	Cyclotetrasiloxane, octamethyl-	0.644	2,3-Pentanedione	0.060
2	2,3-Pentanedione	0.099	Acetoin	0.035
3	Pyridine	0.060	2-Propanone, 1-hydroxy-	0.583
4	Diethyl(3-decyn-1-yl)amine	4.184	2-Pentanone, 4-hydroxy-4-methyl-	0.278
5	2-Propanone, 1-hydroxy-	0.592	1,2-Ethanediol, monoacetate	0.065
6	2-Pentanone, 4-hydroxy-4-methyl-	0.637	Propanoic acid, anhydride	0.147
7	Acetic acid	4.235	4-Methyl-2H-pyran	0.133
8	2-Propanone, 1-(acetyloxy)-	0.521	Acetic acid	3.036
9	3-Furaldehyde	3.944	2-Propanone, 1-(acetyloxy)-	0.404
10	Propanoic acid	0.073	3-Furaldehyde	2.400
11	2-Furancarboxaldehyde, 5-methyl-	0.593	1-Pentanone, 1-(2-furanyl)-	0.187
12	4-Cyclopentene-1,3-dione	0.059	Propanoic acid	0.102
13	Methylenecyclopropanecarboxylic acid	0.574	2-Furancarboxaldehyde, 5-methyl-	0.372
14	Phenol, 2-methoxy-	0.586	4-Cyclopentene-1,3-dione	0.042
15	Phenol	1.037	Methylenecyclopropanecarboxylic acid	0.536
16	Acetic acid, [(aminocarbonyl)amino]oxo-	0.109	Cyclononasiloxane, octadecamethyl-	1.254
17	5-Acetoxymethyl-2-furaldehyde	0.713	2-Cyclopenten-1-one, 2-hydroxy-	0.196
18	Phenol, 2,6-dimethoxy-	0.602	2-Cyclopenten-1-one, 2-hydroxy-3-methyl-	0.093
19	5-Hydroxymethylfurfural	1.912	Phenol, 2-methoxy-	0.612
20			Phenol	0.773
21			Phenol, 4-ethyl-2-methoxy-	0.251
22			Cyclobutanol	0.247
23			5-Acetoxymethyl-2-furaldehyde	0.259
24			Phenol, 5-ethenyl-2-methoxy-	3.151
25			Phenol, 2,6-dimethoxy-	0.739
26			5-Hydroxymethylfurfural	1.215
	Total component	21.18	Total component	17.18

Table S2. Continued

	260 °C		280 °C	
No	Component	HHV	Component	HHV
1	2,3-Butanedione	0.311	2,3-Butanedione	0.230
2	2,3-Pentanedione	0.082	2,3-Pentanedione	0.088
3	2-Propanone, 1-hydroxy-	1.055	Acetoin	0.050
4	2-Pentanone, 4-hydroxy-4-methyl-	0.303	2-Propanone, 1-hydroxy-	1.249
5	1,2-Ethanediol, monoacetate	0.076	1,2,4,5-Tetrazine	0.045
6	Propanoic acid, anhydride	0.181	2-Pentanone, 4-hydroxy-4-methyl-	0.270
7	4-Methyl-2H-pyran	0.270	Acetic acid, (acetyloxy)-	0.094
8	Acetic acid	3.966	Propanoic acid, anhydride	0.218
9	4-Chloro-3-methyl-2-butenyl acetate	0.611	4-Methyl-2H-pyran	0.269
10	2-Propanone, 1-(acetyloxy)-	0.504	2(3H)-Furanone, 5-methyl-	0.073
11	3-Furaldehyde	3.092	Acetic acid	3.912
12	2-Butanone	0.045	Propanoic acid, 2-oxo-, methyl ester	0.274
13	Furan, 2-(dichloromethyl)-tetrahydro-	0.101	2-Propanone, 1-(acetyloxy)-	0.539
14	Propanoic acid	0.203	3-Furaldehyde	2.686
15	2-Furancarboxaldehyde, 5-methyl-	0.565	Furan, 2-(dichloromethyl)-tetrahydro-	0.198
16	2-Cyclopenten-1-one, 3-ethyl-2-hydroxy-	0.295	2,3-dimethylfuran	0.095
17	Methylenecyclopropanecarboxylic acid	1.052	Propanoic acid	0.237
18	2-Cyclopenten-1-one, 2-hydroxy-	0.447	2-Furancarboxaldehyde, 5-methyl-	0.567
19	2-Cyclopenten-1-one, 2-hydroxy-3-methyl-	0.264	Butanoic acid, 4-hydroxy-	0.048
20	Phenol, 2-methoxy-	0.996	3-Hexen-2-one, 5-methyl-	0.124
21	Oxazolidine, 2,2-diethyl-3-methyl-	0.204	Furan, 2-methoxy-	0.098
22	2-Methoxy-5-methylphenol	0.139	Methylenecyclopropanecarboxylic acid	1.070
23	Phenol	1.008	2-Cyclopenten-1-one, 2-hydroxy-	0.624
24	Pentanal	0.393	2-Cyclopenten-1-one, 2-hydroxy-3-methyl-	0.405
25	5-Acetoxymethyl-2-furaldehyde	0.248	Phenol, 2-methoxy-	1.092
26	Phenol, 2,6-dimethoxy-	1.162	2-Cyclopenten-1-one, 3-ethyl-2-hydroxy-	0.147
27	5-Hydroxymethylfurfural	1.695	2-Methoxy-5-methylphenol	0.092
28			Phenol	0.985
29			Phenol, 3-ethyl-	0.169
30			Cyclobutanol	0.379
31			5-Acetoxymethyl-2-furaldehyde	0.141
32			Phenol, 2,6-dimethoxy-	1.353
33			3-acetyl-3-methyl-.gamma.-butyrolactone	0.113
34			1,4:3,6-Dianhydro-.alpha.-d-glucopyranose	0.175
35			5-Hydroxymethylfurfural	1.330
	Total component	19.28	Total component	19.45